VOL. 16, NO. 19, OCTOBER 2021 ISSN 1819-6608
ARPN Journal of Engineering and Applied Sciences

www.arpnjournals.com

SPECTRAL IMAGE CLASSIFICATION FROM COMPRESSIVE MEASUREMENTS BASED ON SINGULAR VALUE DECOMPOSITION

Ferley Medina Rojas[1], Juan A. Castro Silva[1] and Faiber Robayo Betancourt[2]
[1]Departamento de Ingeniería de Software, Facultad de Ingeniería, Universidad Surcolombiana, Neiva, Huila, Colombia
[2]Departamento de Ingeniería Electrónica, Facultad de Ingeniería, Universidad Surcolombiana, Neiva, Huila, Colombia
E-Mail: ferley.medina@usco.edu.co

ABSTRACT

Classification consists of categorizing image pixels, specifically, in a spectral image (SI) it is used to determine environmental pollution agents, to stable land use, and to monitor crops. Due to the high dimensionality of the SI, classification is inefficient. However, compressive sampling (CS) has been established as a sampling protocol of SI allowing the reduction of data. Recently, CS classification is a promising research area, but it has only been tested on some specific systems. This paper proposes a general classification algorithm in compressive spectral imaging which uses singular value decomposition for estimating sparse dictionary of the data. From this dictionary, the algorithm performs a rough estimation which allows the classification of every spectral pixel in known classes by using discriminant analysis. The estimation is made by solving the inverse problem. Simulations with three state of the art compressive imagers show the outstanding performance of the proposed algorithm even in presence of noise.

Keywords: classification, compressive sampling, spectral imaging, compressive spectral imaging.

1. INTRODUCTION

In hyperspectral imaging, the sensors measure the electromagnetic energy scattered in their instantaneous field view in hundreds or thousands of spectral channels. The very high spectral resolution of hyperspectral images enables a precise identification of the sensed materials via spectroscopic analysis, facilitating countless applications; e.g., earth observation and remote sensing, food safety, pharmaceutical process monitoring and quality control, as well as biomedical, industrial, and forensic applications. The extraction of useful information from hyperspectral images calls for sophisticated inference methods. The sources of difficulties are, for instance, the high dimensionality and size of hyperspectral data, spectral mixing, and other degradations, such as noise and atmospheric effects. The tackling of these difficulties corresponds to one of the inverse problems, namely hyperspectral unmixing, denoising, compressive acquisition, segmentation, and classification.

Specifically, classification is used to categorize each pixel in an image, that is to distinguish between $\mathbf{H}(\mathbf{S}_0 + n)$ and $\mathbf{H}(\mathbf{S}_1 + n)$ defined by the hypothesis H_i : $\mathbf{g} = \mathbf{H}(\mathbf{f}_i + n)$, for i= 1,2,..,R, where $\mathbf{f}_i$ is the known signal, with $\mathbf{f}_i \in \mathbf{S}$, $R = |\mathbf{f}|$, and $\mathbf{S}$ are the classes.

Several techniques have been used to perform supervised classification of hyperspectral data. For instance, in discriminant classifiers, several types of discriminant functions can be applied: nearest neighbor, decision trees, linear functions, non-linear functions, etc. In linear discriminant analysis (LDA) [1], a linear function is used in order to maximize the discriminatory power and separate the available classes effectively. However, such a linear function may not be the best choice and nonlinear strategies such as quadratic discriminant analysis (QDA) or logarithmic discriminant analysis (LogDA) have also been used. The main problem of these classic supervised classifiers, however, is their sensitivity to the Hughes effect. In this context, kernel methods such as the support vector machine (SVM) have been widely used in order to deal effectively with the Hughes phenomenon [2], [3].

Recently, compressive sampling (CS) has been established as an SI sampling protocol. CS theory efficiently performs signal sampling by reducing redundancy measures exploiting its correlation [4]. Imagers such as Spatial-Spectral Encoded Compressive Hyperspectral Imager (SSCSI) [5], Snapshot colored compressive spectral imager (SCCSI) [6], and also frameworks for compressing spectral images such as Hyperspectral coded aperture (HYCA) [7] have been developed from CS theory. Even, there are classification algorithms of compressed spectral images acquired by using a (CASSI) system [8], [9].

In compressive hyperspectral imaging, the acquisition, and the data compression are implemented simultaneously by computing a number of projections, termed measurements, of the original data onto a set of predesigned vectors. Assuming that the original data admits a sparse representation over a given basis or frame, it can be recovered from the projections by solving a suitable optimization problem.

The success of compressive hyperspectral imaging stems from the very high spectral and spatial correlation of this type of data, meaning that it is compressible, i.e., it admits a representation onto a given frame on which most of the coefficients are small and, thus, it is well approximated by sparse representations. Due to the huge number of optimization variables involved in a typical compressive hyperspectral imaging problem, the solutions of these optimization problems are very demanding from the computational point of view. To make the problem even more challenging, the sparse

representations are not known beforehand and have to be learned from the measurements.

This paper proposes a spectral imaging classification algorithm that acts over compressed measurements for classifying spectral signatures. The approach is based on the fact that the measurements represent sufficiently well the image onto a low-dimensional subspace. There is a general approach for classification on the compressed domain, taking into account measurements from several compressive imagers. Then, the algorithm uses singular value decomposition for estimating sparse representation of the data. From the sparse dictionary, the algorithm performs a rough estimation which allows the classification of every spectral pixel in known classes by using discriminant analysis. The simulation results demonstrate the efficiency of the algorithm on two real datasets and comparability with approaches that use all the data.

2. COMPRESSIVE SPECTRAL IMAGERS BACKGROUND

The measurement model assumes that the hyperspectral image is a column vector of the form $\mathrm{f} = \{\mathrm{f} \in \mathbb{R}^{M\cdot N\cdot L} | [f_1, \ldots, f_{M\cdot N}, \ldots, f_{M\cdot N\cdot L}]^T\}$, where M and N represent the spatial resolution and L the spectral resolution; f can also be expressed by $\mathrm{f} = \Psi^T \mathrm{s}$, where $\mathrm{s} \in \mathbb{R}^{M\cdot N\cdot L}$ contains only $S \ll M \cdot N \cdot L$ nonzero elements and $\Psi \in \mathbb{R}^{M\cdot N\cdot L\times M\cdot N\cdot L}$ is a sparsifying operator. The measurements vector $\mathrm{g} \in \mathbb{R}^q$ is obtained as $\mathrm{g} = \mathrm{Hf}$, where $\mathrm{H} \in \mathbb{R}^{q\times M\cdot N\cdot L}$ is a sensing matrix. By choosing the number q projections and H and assuming sparsity of f in the Ψ domain, the signal f can be recovered from model $\mathrm{g} = \mathrm{H}\Psi^T s$.

Compressive sensing imagers are usually model by coded projection operator whose entries are related to the sampling patterns. For instance, the CASSI System uses a coded aperture to replace the entrance slit of a dispersive spectrometer with a much wider field stop, inside which is inserted a binary-coded mask. This mask attempts to create a transmission pattern. The encoded light, transmitted by the coded mask within the field stop, is then passed through a standard spectrometer back-end (i.e., collimating lens, disperser, reimaging lens, and detector array). Thus, the sparse modulation matrix has binary entries, such as is shown in Figure-1, note that its structure consists of a set of diagonal patterns, that repeat along the horizontal direction, such that one spatial dimension is shifted downward, as many times as the number of spectral bands. Each diagonal element is due to the sampling pattern that has been vectorized column-wise. Other patterns of diagonal elements are vertically stacked when several snapshots are considered by the system.

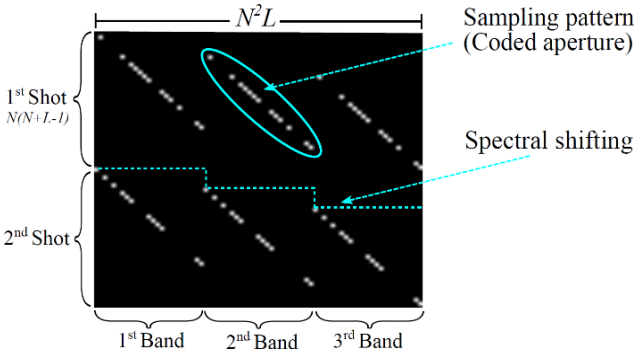

Figure-1. Compressed sample matrix of the compressive architecture, N=3, L=3, and 2 shots, $H_{CASSI} \in \mathbb{R}^{(N(N+L-1))q\times N^2L}$.

On the other hand, the SSCSI employs a diffraction grating to disperse light into the spectral plane and adopt a coded attenuation mask mounted at a slight offset in front of the sensor. The mask modulates the target HS images in both spatial and spectral dimensions before projection into a sensor image. A compression procedure with spectral coding is shown in Figure-2. Note that its structure also consists of a set of diagonal patterns, but it does not repeat horizontally, allowing to perform spectral coding.

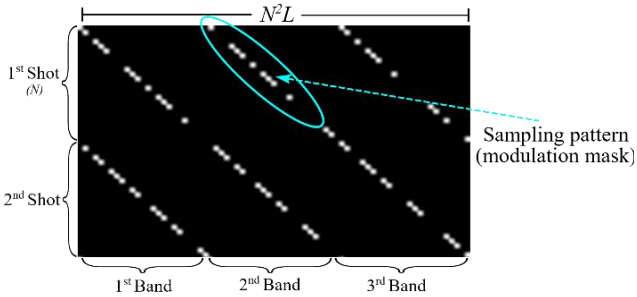

Figure-2. Compressed sample matrix of the compressive architecture, N=3, L=3, and 2 shots, $H_{SSCSI} \in \mathbb{R}^{N^2q\times N^2L}$.

Finally, there are some theoretical approaches, without physical implementation that compute a few random projections using, for instance, Gaussian independent identically distributed (i.i.d.) vectors based on the approaches of physical spatial/spectral coding (see [7]), for the success of data recovery.

3. MATERIALS AND METHODS

3.1 Subspace Spectral Image Classifications

Hyperspectral imaging is characterized by the high spectral resolution available, which allows capturing fine details of the spectral characteristics of materials in a wide range of applications. However, it has been demonstrated that the original spectral features contain high redundancy. Specifically, there is a high correlation between adjacent bands and the number of the original spectral features may be too high for classification purposes. It is that spectral images lying on a low

dimensional subspace, built from the singular value decomposition.

3.2 Sparse Dictionary Building

The singular value decomposition (SVD) of a matrix **A** is very useful in the context of least squares problems. It is also very helpful for analyzing the properties of a matrix. Currently, used An intelligent and blind image watermarking scheme based on hybrid SVD transforms using human visual system characteristics [12], A block-based RDWT-SVD image watermarking method using human visual system characteristics [13].

Let **A** be an $m \times n$ matrix with $m \leq n$. Then there exist orthogonal matrices $\mathbf{U} \in \mathbb{R}^{m \times m}$ and $\mathbf{V} \in \mathbb{R}^{n \times n}$ and a diagonal matrix $\Sigma = \text{diag}(\sigma_1, \cdots, \sigma_n) \in \mathbb{R}^{m \times n}$ with $\sigma_1 \leq \sigma_2 \leq \sigma_n \leq 0$, such that

$$\mathrm{A} = \mathrm{U}\Sigma\mathrm{V}^T \quad (1)$$

holds. If $\sigma > 0$ is the smallest singular value greater than zero then the matrix **A** has rank r. The column vectors of $\mathbf{U} = [\mathbf{u}_1, \cdots, \mathbf{u}_m]$ are called the left singular vectors and similarly $\mathbf{V} = [\mathbf{v}_1, \cdots, \mathbf{v}_n]$ are the right singular vectors. The values σ_i are called the singular values of **A**.

We propose to use the left singular vectors to create a basis, the projections over that basis represent the data sufficiently well, and it is compressible. This fact that is a needed in compressive sensing approaches. Figure-3 shows an example of a spectral pixel projected over the left singular vectors of a selection of training samples, the performance of the curve indices the capability to represent the power of the signal [14].

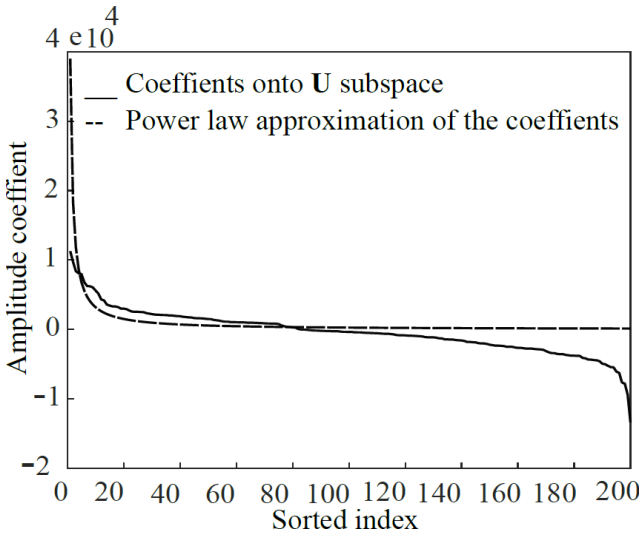

Figure-3. Curve or intensities of a spectral pixel projected on singular vectors. The curve indicates the ability to represent the signal potency.

Then, a dictionary is built from the matrix **U** as the linear combination

$$\mathrm{D} = \mathrm{UT} \quad (2)$$

where **T** contains a selection of the pure spectral components (endmembers). There is assumed the knowledge of the signatures of the endmembers to be more precise to represent the spectral vectors. For taking into account that the smoothness is a feature present in the images, it is included a parameter promoting the spatial interpixel correlation as the Kronneker product $\widehat{\mathbf{D}} = \mathbf{D} \otimes \mathbf{\Omega}_{2D}$, with $\mathbf{\Omega}_{2D}$ as a wavelet kernel.

3.3 Rough Estimation

The dictionary allows estimating sparse vectors, which represents the data (sufficiently well). Then the process consists of computing a rough estimation of a sparse vector on the $\widehat{\mathbf{D}}$ domain from the compressed measurements **g**. We assume that the stimulation are sufficient to depict the data and allows classification of the known observations in the domain of the images. The estimation can be performed by solving the inverse problem

$$\hat{\mathbf{s}} = \min_{\mathbf{s}} ||\mathbf{s}||_0 \text{ s.t. } \mathbf{g} = \mathbf{H}\widehat{\mathbf{D}}\mathrm{s} \quad (3)$$

where **s** is the sparse representation of **f** onto the $\widehat{\mathbf{D}}$ subspace. Note that the problem is the same to recover the image from the observation, but here, the result is a representation of the compressed signatures of the endmembers. This problem can be solved by different approaches, specifically, we use the gradient descent method, and the algorithm gradient projection for sparse reconstruction (GPSR) algorithm, which is widely used in this type of problems. Note that the estimation also corresponds to a representation of the compressive measurements, in the same domain that the image has low dimensionality.

3.4 Pixel Classification

For the pixel classification purposes, the rough estimation is used as a sample to be tested instead of pure compressive measurements. The class of a given pixel is found as:

$$\mathrm{C} \leftarrow \min_{\lambda=1,\ldots,\Lambda} ||\hat{\mathrm{s}}_i - \mathrm{s}_{(\lambda)}||_2^2 \quad \forall \quad i = 1, \cdots, MNL$$

where $\mathbf{s}_\lambda$ correspond to training samples, which are compared to the test samples from the rough estimation **s**. Notice that the least square attempt to test every spectral pixel with the known classes to decide its correspondence. This procedure is clarified in [8]. In summary, the proposed procedure to classify the observations with compressive spectral imagers is presented in the algorithm 1 and Table-1 shows the variables.

Algorithm 1 Classification of HSI from compressive measurements
Inputs: g, H, $S = S_{(1)}, S_{(2)}, \dots, S_{(\Lambda)}$, ρ, Ψ, s Output: C
1. Singular value decomposition $A = U\Sigma V^T$
2. Create sparsifying basis $D = UT$ $\widehat{D} \leftarrow D \otimes \Omega$
3. Estimation of sparse vector in the PCA domain from the compressive measurements $\hat{s} \leftarrow \Omega^T \{ \min_s (\| g - H\overline{\Psi} s \|_2^2 + \tau \| s \|_1 \}$
4. Test pixels classifications $C \leftarrow \min_{\lambda=1,\dots,\Lambda} \|\|\hat{s}_i - s_{(\lambda)}\|\|_2^2 \quad \forall \quad i = 1, \cdots, MNL$

Table-1. Summary of variables.

variable	size	Description
g	**M(N+L-1)**	**compressive measurements**
H	M(N+l-1) x MNL	measurement matrix
S	Λ	Classes
ρ	scalar	data learning %
$\overline{\Psi}$	MNL ×MNL	sparse basis
s	MNL	sparse representation of **F** in **Ψ**
Ψ	NML × NML	sparse dictionary
Ω	NML × MNL	wavelet basis
τ	scalar	regularization parameters
$\hat{s}$	MNL	test sample
$s_{(\lambda)}$	MNL	training sample
c	Λ	classified pixels

4. RESULTS AND DISCUSSIONS

The compressive imagers have been considered to generate the measurements **g**. All systems consider the same HS image, which is compressed by the operator how in Figure 3. The original spectral HS image is the classical Indian Pines image acquired over North-western Indiana [15]. The Indian Pines scene contains two-thirds agriculture, and one-third forest or other natural perennial vegetation. Another image has been tested, the Salinas scene image, this image was acquired over Salinas Valley, California [16]. Both acquired by the AVIRIS sensor. The reference images were reduced to 128×128 pixels and 200 bands. Thus the compressed measurements were simulated by using the CASSI, SSCSI, and HYCA operators. The value of τ was selected by cross-validation and we found that the interval [1e-2, 1e-3] provides good and similar results for the image classification.

The first experiment attempt to select a compression ratio that promotes good results on classification, Table-2 gives the general results for the compression ratio evaluation with CASSI, SSCSI, and HYCA. We can observe that the classification amount increases as the compression ratio increases, as expected. The best compression rate is 38%, only 0.63% of classification is lost compared to the compression rate of 50%, where it obtained the highest classification.

Table-2. Classification results for the spectral imagers.

C%	Clas. % Indian Pines			Clas. % Salinas		
	CASSI	SSCSI	HYCA	CASSI	SSCSI	HYCA
25	61,47	65,10	65,33	84,00	86,00	86,23
38	65,19	69,13	69,36	88,84	89,24	89,87
50	70,67	73,18	73,41	88,94	90,03	90,50

Table-3 shows the classification results in terms of the number of classes, a compression ratio of 38%. Figures 4 and 5 compares the performance of the approach in the presence of noise for a compression ratio of 38%, as a function of the signal to noise ratio (SNR) defined as $SNR = 10\log_{10}(\mu_y/\sigma_{noise})$, where μ_y is the mean value of the measurement vector y and σ_{noise} is the noise standard deviation. Despite the loss in classification performance, the proposed approach provides close to 64,89% and 84,87% of classification for $SNR \geq 20$ dB, which is very promising.

Table-3. Classification results for the spectral imagers.

Classes	Classification % Indian Pines			Classification % Salinas		
	CASSI	SSCSI	HYCA	CASSI	SSCSI	HYCA
1	16,67	11,11	11,11	99,73	99,83	99,88
2	61,44	69,80	72,38	96,80	98,45	98.67
3	32,21	32,69	40,38	99,58	99,67	99,83
4	53,42	55,98	52,56	95,65	97,56	97,74
5	54,73	64,59	67,81	29,37	31,59	31,81
6	97,46	98,66	97,19	96,30	98,35	98,84
7	11,54	11,54	11,54			
8	95,03	96,69	89,50			
9	10,00	10,00	10,00			
10	49,02	33,60	32,33			
11	77,96	88,53	87,93			
12	40,23	32,57	25,41			
13	32,08	61,79	82,08			
14	90,11	86,53	81,83			
15	51,58	62,89	67,37			
16	57,89	78,95	80,00			
Total	65,19	69,13	69,36	88,84	89,24	89,87

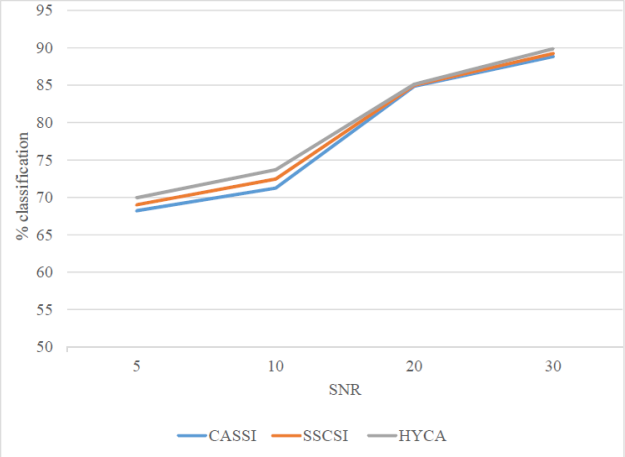

Figure-4. Classification results in Salinas dataset white noise.

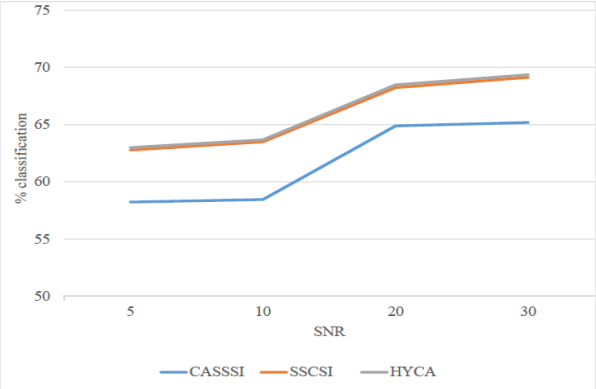

Figure-5. Classification results in Indian dataset white noise.

The last simulation results displayed in Figures 6 and 7 show that the proposed classification method provides a closed result to the ground truth.

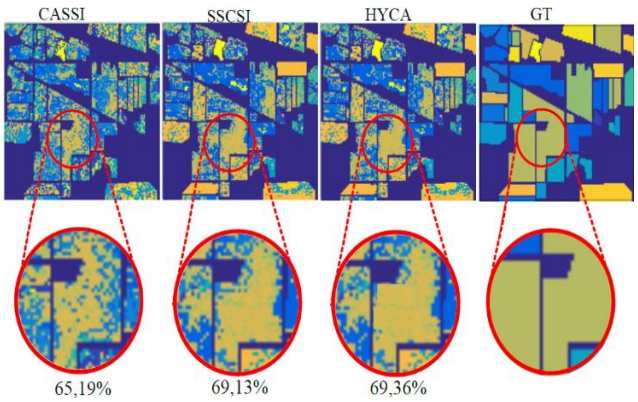

Figure-6. Classification results in Indian Salinas dataset.

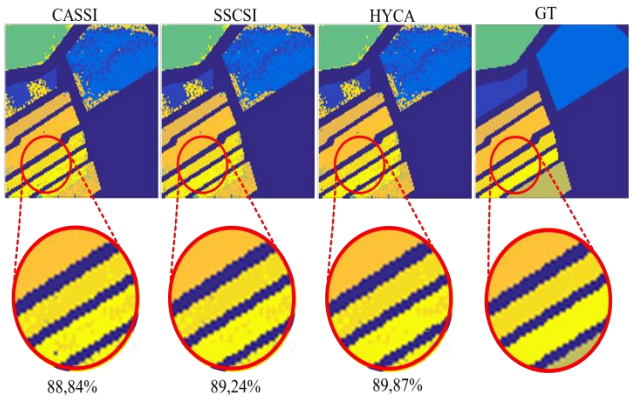

Figure-7. Classification results in Salinas dataset.

5. CONCLUSIONS

In this work, an approach was evaluated that allows us to classify the spectral images, acquired by compressive sensing-based imagers. It presented a comparison between the different kinds of CS imagers, with three representative architectures, such as CASSI, SSCSI, and HYCA framework. As expected, the best results were obtained by using the HYCA framework. Specifically, the results of classification achieved were 65,19% for the CASSI system, 69,13% for the SSCSI system and 69,36% for the HYCA framework, by using just approximately 38% of the data. The idea of our approach is to establish a general framework to classify spectral images from the compressed measurements acquired with the different CS imagers, taking into account, the structure of the sensing matrices, respectively.

REFERENCES

[1] Ye Qiaolin, Ye Ning and Yin Tongming. 2015. Fast orthogonal linear discriminant analysis with application to image classification. Neurocomputing. 158: 216-224.

[2] Lianru Gao, Jun Li, Khodadadzadeh M, Plaza A, Bing Zhang, Zhijian He and Huiming Yan. 2015. Subspace-Based Support Vector Machines for Hyperspectral Image Classification. Geoscience and Remote Sensing Letters, IEEE. 12(2): 349-353.

[3] P. Ghamisi, M. Dalla Mura and J. A. Benediktsson. 2015. A Survey on Spectral–Spatial Classification Techniques Based on Attribute Profiles. IEEE Transactions on Geoscience and Remote Sensing. 53(5): 2335-2353.

[4] Baraniuk Ricard G. 2007. Compressive Sensing [Lecture Notes]. IEEE Signal Processing Magazine. 24(4): 118-124.

[5] X. a. L. Y. a. W. J. a. D. Q. Lin. 2014. Spatial-spectral encoded compressive hyperspectral imaging. ACM Trans. Graph. 33(6): 233: 1-233: 11.

[6] Correa, C. V. A. and Arguello, H. b and Arce, G. R. A. 2014. Compressive spectral imaging with colored-patterned detectors. In ICASSP, IEEE International Conference on Acoustics, Speech and Signal Processing - Proceedings. pp. 7789-7793.

[7] Martin Gabriel, Bioucas-Dias, Jose M and Plaza, Antonio. 2015. HYCA: A New Technique for Hyperspectral Compressive Sensing. IEEE Transactions on Geoscience and Remote Sensing. 53(5): 2819-2831.

[8] Ramirez, Ana and Arguello, Henry and Arce, Gonzalo R. and Sadler, Brian M.. 2014. Spectral image classification from optimal coded-aperture compressive measurements. IEEE Transactions on Geoscience and Remote Sensing. 52(6): 3299-3309.

[9] H. A. A. G. Arguello. 2010. Code aperture design for compressive spectral imaging. In 18th European Signal Processing Conference, Aalborg. pp. 1434-1438.

[10] M. R. Ferley, A. F. Henry and G. S. Cristina. 2017. A quantitative and qualitative performance analysis of compressive spectral imagers. Tecnura, 21(52). http://dx.doi.org/10.14483/udistrital.jour.tecnura.2017.2.a04, pp. 53-67.

[11] C. Zhen, H. Chuanping and L. Shufu. 2019. A new sparse representation framework for compressed sensing MRI. Knowledge-Based Systems, vol. 188, no. 5 https://doi.org/10.1016/j.knosys. pp. 1-10.

[12] B. B. A. Sajjad, Z. Gongxuan, W. Songjie, and B. Lynda. 2020. An intelligent and blind image watermarking scheme based on hybrid. The Visual Computer, no. https://doi.org/10.1007/s00371-020-01808-6, pp. 1-25.

[13] F. Ernawan and M. A. Kabir. 2018. A block-based RDWT-SVD image watermarking method using human visual system characteristics. The Visual Computer, vol. 36, no. https://doi.org/10.1007/s00371-018-1567-x, pp. 19-37.

[14] Duarte, Marco F. and Hegde, Chinmay and Cevher, Volkan and Baraniuk, Richard G. 2009. Recovery of compressible signals in unions of subspaces. In Proceedings - 43rd Annual Conference on Information Sciences and Systems, CISS, Baltimore, MD. pp. 175-180.

[15] Indiana's, AVIRIS NW. 1992. Indiana's Indian Pines Dataset.

[16] (UPV/EHU). 2014. Grupo de Inteligencia Computacional de la Universidad del Pais Vasco, "Hyperspectral Remote Ssensing Scenes.